KSCE Journal of Civil Engineering (2020) 24(7):2120-2131
DOI 10.1007/s12205-020-1970-5

pISSN 1226-7988, eISSN 1976-3808
www.springer.com/12205

Structural Engineering

Life Prediction and Long-Term Durability of Coated Steel Bars in Magnesium Oxychloride Concrete

Penghui Wang[a], **Hongxia Qiao**[a,b], **Kefan Chen**[a], **Yuanke Li**[a], **and Qiong Feng**[a]

[a]*Key Laboratory of Disaster Prevention and Mitigation in Civil Engineering of Gansu Province, Lanzhou University of Technology, Lanzhou 730050, China*
[b]*Qinghai Institute of Salt Lakes, Chinese Academy of Sciences, Xining 810008, China*

ARTICLE HISTORY

Received 30 October 2019
Revised 27 February 2020
Accepted 22 March 2020
Published Online 1 June 2020

KEYWORDS

Long-term durability
Solution immersion accelerated test
Polarization curve
AC impedance
Wiener function
Life prediction

ABSTRACT

The solution to the problem of corrosion of the steel bars in magnesium oxychloride cement concrete (MOCC) is to apply a coating that protects the steel. To investigate the coating's long-term protective effect on the steel, a solution immersion accelerated corrosion test was carried out on coated reinforced MOCC for up to 2,160 days. Electrochemical tests were conducted every 90 days to measure the polarization curve and AC impedance during the steel bars' corrosion process. Then, the corrosion current density that characterizes the corrosion of a coated steel bar was used as a degradation index, and the time to the coated steel bar's corrosion was predicted based on the Wiener function. It was concluded that after 2,160 days of solution immersion, the coated steel bars' corrosion current density was 0.063 μA·cm^{-2}, indicating that the coating protected the steel bars in MOCC from corrosion well. Thdroughout the immersion process, the specimen's corrosion current density showed a steady and increasing trend, and its polarization impedance showed a volatile growth trend. The degradation of the coated steel bars also obeyed the Wiener degradation process, and the bars reached a severely rusted state at 21,800d with a corrosion time of $R_{0.6}(t)$ is 10,650d.

1. Introduction

Because of the large amount of sulfate and chloride in the soilin saline soil areas, ordinary reinforced concrete does not have good applicability, and damage usually occurs within 3 – 5 years (Ma et al., 2018; Qiao et al., 2018). The reason that ordinary reinforced concrete fails is the corrosion of steel that chloride causes, while sulfate causes the concrete to fail (Tang et al., 2016; O'Reilly et al., 2018; Mohabbi, 2019; Sotiriadis and Mróz, 2019). The typical solutions used are to modify the concrete or improve the steel bars' corrosion resistance, so that the concrete is more durable. The methods used to improve the durability of concrete are as follows:

For example, high-performance concrete and ordinary concrete are subjected to dry-wet cycling, and then X-ray diffraction analysis is carried out. The results show that the salt-halogen resistance of high-performance concrete is clearly greater than that of ordinary concrete, and the damage to ordinary concrete is the greatest in Qinghai Lake (Ma et al., 2018). Jin et al. (2007) carried out the solution immersion test and dry-wet cycle test on plain concrete and fly ash concrete with 20% and 30% content of sulfate, chloride, and compound salt solution, respectively, and concluded that fly ash can improve concrete's corrosion resistance to sulfate and chloride. Niu simulated the initial lining of tunnel by dry-wet cycling method, and carried out the durability test of shotcrete under a compound salt solution (sulfate, chloride, magnesium salt). Thereafter, the corrosion products and microstructure were analyzed by bothmicro-andmacro-tests. The results showed that steel fiber improved the shotcrete's durability (Wang et al., 2018). Zhang et al. (2019) carried out carbonation curing on concrete, and then tested the steel's loss of quality, and the concrete's porosity, chloride ion content, and compressive strength. The results showed that carbonation curing improved not only the early strength of the concrete, but also reduced the penetration of chloride ions in the concrete and the steel's loss of quality significantly. Yehia et al. (2019) added fiber to concrete to improve its durability, and circulated the fiber-reinforced concrete in salt water for one year. The compressive

CORRESPONDENCE Hongxia Qiao qiaohongxia@lut.edu.cn Key Laboratory of Disaster Prevention and Mitigation in Civil Engineering of Gansu Province, Lanzhou University of Technology, Lanzhou 730050, China; Qinghai Institute of Salt Lakes, Chinese Academy of Sciences, Xining 810008, China

strength, flexural strength, and elastic modulus were calculated, and scanning electron microscopy (SEM) and the rapid chloride ion penetration test (RCPT) were carried out on the specimen. The author found that the fiber changed the concrete's microstructure, but did not increase the chloride ion permeability, while the compressive strength, flexural strength, and crack resistance improved significantly.

Steel protection is achieved primarily by increasing the protective layer on the steel surface or adding other metal elements to make the steel more corrosion resistant. For example, Xiong et al. (2018) used phytic acid conversion coating in a Zn^{2+}-doped phytic acid (PA-Zn) solution at 20°C to improve the corrosion resistance of steel bars in concrete. Ohba et al. (2019) used hot dip galvanizing, electroplating, or thermal spraying to form a galvanized metal layer on the surface of the steel bar to protect it, and found that the galvanized steel bar's corrosion resistance improved significantly. Fajardo et al. (2019) carried out a solution immersion test on High-Mn austenitic twinning-induced plasticity (TWIP) steels and TWIP. Through electrochemical analysis, he concluded that High-Mn TWIP steel has greater corrosion resistance than does TWIP steel. The research above has demonstrated that the primary way to improve concrete's durability is to change the curing method, add modifying materials, and use corrosion-resistant steel bars. However, using the methods above results in a significant increase in production costs. Magnesium oxychloride cement concrete (MOCC) as a kind of magnesia cementitious material ($MgO\text{-}MgCl_2\text{-}H_2O$), its binder after hardening is $5Mg(OH)_2 \cdot MgCl_2 \cdot 8H_2O$ and $3Mg(OH)_2 \cdot MgCl_2 \cdot 8H_2O$, resists salt brine very well without modification. Therefore, compared with ordinary concrete, it is more applicable in saline soil areas, is not damaged by sulfate erosion (Li and Chau, 2007; Chau et al., 2009; Tan et al., 2014; Hu et al., 2016), and its production cost is low. The main degradation is attributable to the accelerated effect of internal and external chloride ions on the steel, which causes the steel to rust and the concrete to crack in a short time (Skalny, 2000; Wei et al., 2018; Wang et al., 2019). In view of the corrosion of steel bars in MOCC, Gong applied a coating on the surface of the steel bar, carried out the solution immersion test on the test piece, and found that the coating prevented the corrosion of the steel bar well (Gong, 2017). However, a short-term durability test of only 720 days was carried out on the coated steel bars.

Clearly, research has demonstrated that a coating can protect steel from corrosion. However, the corrosion of steel in concrete is a long-term process, and whether a coating can provide long-term and stable protection for the steel is still worthy of further study. To the best of my knowledge, no relevant research has conducted a 2,160 days solution immersion test on coated reinforced MOCC to study the coating's long-term stability. However, a long-term tracking study is expensive, so an effective method must be used to evaluate the coating's long-term protective performance. As a method of reliability modeling and prediction, the Wiener degradation process is used widely in reliability modeling because it can describe the degradation process in a product's performance and has good computational and analytical properties. For example, Sun et al. (2018) used Wiener to predict the residual life of cutting tools, Zhang et al. (2018) used it for prognostics and health management (PHM), Hu et al. (2018) used Wiener to predict the life of wind turbine bearings, Li et al. (2019) used it to predict the life of a machine, and so on. However, the application of the Wiener degradation process to life prediction of coated steel bars has not been studied yet. Therefore, this paper presents the results of a long-term (2,160 days) solution immersion accelerated corrosion test for coated reinforced MOCC. Electrochemical tests of the coated reinforced MOCC were carried out regularly. Then, the corrosion current density was measured, and used as the corrosion degradation index of coated steel bars, and based on the Wiener degradation process, the corrosion time of coated steel bars was predicted.

2. Experiment

2.1 Experimental Materials

The raw materials of MOCC concrete are composed largely of light-burned magnesium oxide (MgO), magnesium chloride ($MgCl_2$), a water reducing and water repellent agent, fly ash, sand, gravel, and steel bars. Both MgO and $MgCl_2$ are produced by Qarhan Salt Lake Magnesium chloride plant, Golmud City, Qinghai Province. Well graded, medium level river sand was obtained from Shuifu, Lanzhou. Gansu Hualong Concrete Co., Ltd. provided the gravel, which had a continuous gradation and qualified performance indicators. A steel mill in Lanzhou produces the I grade fly ash used in this study to improve the concrete's durability. The water-proofing agent was phosphoric acid from Tianjin Baishi Chemical Co., Ltd. The H_3PO_4 content was no less than 85%, and the Hazen Unit was less than 25. Jiangsu Bote New Material Co., Ltd. produced the water-reducing agent in the KD naphthalene series with high efficiency (JM-PCA(I)) that was used. The basic physical properties are shown in Table 1. The tap water used was consistent with the industry standard and requirements of the "Standard specification for concrete mixing water" JGJ63-2006 (2018). An HPB300 steel bar was employed, the yield strength of which was f_y = 300 N/

Table 1. The Physical Indicators of the Water Reducing Agent

Species	Density value/g/ml	PH	Alkali content/%	Water reduction rate/%	Bleeding rate/%	Compressive strength ratio			Recommended dosage%
						3d	7d	28d	
PCA(I)	0.0003	8.08	≤ 3.88	34	0	168	149	139	0.02

Table 2. Mixing Proportion of Magnesium Oxychloride Cement Concrete (kg/m^3)

MgO/ (kg/m^3)	Water reducer/ (kg/m^3)	Water repellent/ (kg/m^3)	Sand/ (kg/m^3)	Cobblestone/ (kg/m^3)	$MgCl_2$/ (kg/m^3)	Water/ (kg/m^3)	Slum/ (mm)
388.96	2.288	1.6016	625	1162	147.811	135.586	120

mm^2. Ningbo Metal Surface Treatment Co., Ltd. provided the Japan's GEOMET coating (a type of zinc coating that includes a large number of ultrafine zinc-aluminum flakes).

2.2 Specimen Preparation

The HPB300 steel bar was 100 mm in length with a diameter of 8 mm. The steel bar was cleaned by washing with acid and alkali to remove surface oil pollution in preparation to coat the bar. According to the mixing ratio in Table 2, MOCRC with a concrete protective layer of 46 mm was prepared with a test piece size of 100 mm × 100 mm × 100 mm.

2.3 Experimental Study

To investigate the long-term effect of the protective coating on the steel, the specimen was subjected to a solution immersion accelerated corrosion test, and the electrochemical test was performed periodically. The specific test method is as follows:

2.3.1 Accelerated Test of Solution Immersion

The test blocks were divided into two groups of three blocks according to their surface, group A (uncoated steel bar) and group B (coated steel bar). The test blocks were placed in a magnesium oxychloride solution with a chloride ion concentration of 1.5 mol/L, where the height of the solution was 2/3 of the block.

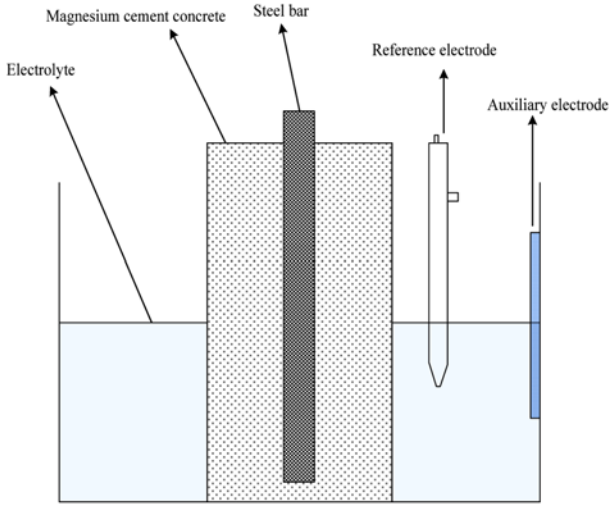

Fig. 1. Schematic Diagram of Three-Electrode System

2.3.2 Electrochemical Test

The test system in the electrochemical test is a three-electrode test system, the schematic diagram of which is shown in Fig. 1. The electrolyte of group A was water, and that of group B was magnesium oxychloride solution with a chloride ion concentration of 1.5 mol/L. Before the electrochemical test in group A, the specimens were immersed for 1 day to form a better circuit, and thereafter, the benchmark test was performed with the Zahner electrochemical workstation. Coated steel with an area of 25.12 cm^2 served as the working electrode. A thin stainless-steel plate with an area of 30 cm^2—greater than that of the working electrode—served as an auxiliary electrode, while a saturated KCl electrode served as the reference electrode. An electrochemical test was performed on the test block every 90 days after the benchmark test. The relation between the corrosion current density and the steel bar's corrosion is shown in Table 3. The scanned range of the polarization curve was from -0.2 mV to 0.2 mV of the relative corrosion potential, the scanning rate was 334 μV/s, and the current range was -1 – 1 μA. The range of the AC impedance measurement frequency was 0.01 Hz – 100,000 Hz, the AC positive rotation excitation signal amplitude was 10 mV, and the AC impedance test used metal shielding as electromagnetic shielding.

In the corrosion system used to control the activation polarization, the basic formula of the polarization current density, I, and the electrode potential, E, are shown below:

$$I = i_{corr}\left\{\exp\left[\frac{2.3(E-E_{corr})}{b_a}\right]-\exp\left[\frac{2.3(E_{corr}-E)}{b_c}\right]\right\} \quad (1)$$

$$b_a = \frac{2.303RT}{\beta_a nF} \qquad b_c = \frac{2.303RT}{\alpha_c nF} \quad (2)$$

in which i_{corr} is the natural corrosion current density that represents the corrosion rate in the electrochemical corrosion. E is the electrode potential, E_{corr} is the natural corrosion potential, R is the gas constant, T is the absolute temperature, F is the Faraday constant, b_a and b_c are the transfer coefficients of the anodic and cathodic reactions, n is the number of electrons gained or lost for the electric polar reaction speed control step, and β_a and α_c are Tafel's anodic and cathodic slopes.

Impedance is a vector that can be expressed as a complex number. A complex number consists of real and imaginary elements. The real element is the component of the vector in the

Table 3. The Corresponding Relation between Corrosion Current Density and the Degree of the Rebars' Corrosion

i_{coor} / (μA·cm^{-2})	$i_{coor} < 0.1$	$0.1 < i_{coor} < 0.5$	$0.5 < i_{coo}r < 1$	$i_{coor} > 1$
Corrosion situation	No corrosion	Low corrosion	Medium corrosion	Serious corrosion

horizontal coordinate, and the imaginary element is that in the vertical coordinate. In electrochemistry, the coordinate system includes $-Z''$ (the vertical axis) and Z' (the horizontal axis), which represents the impedance plane.

$$Z = Z' - jZ'' \tag{3}$$

$$Z' = |Z|\cos\theta \quad Z'' = |Z|\sin\theta \tag{4}$$

$$|Z| = \sqrt{Z'^2 + Z''^2} \quad tg\theta = \frac{Z''}{Z'} \tag{5}$$

where Z' is the real element of the impedance, $-Z''$ is the imaginary element, $|Z|$ is the impedance of the module, and θ is the impedance angle, $j = (-1)^{1/2}$:

When the resistance element, C, is connected in series with the capacitance element, R.

$$Z = R - j\frac{1}{\omega C} \tag{6}$$

When the resistance element, C, is connected in parallel with the capacitor element, R.

$$Z = Z' - Z'' = \frac{R}{I + (\omega RC)^2} - j\frac{\omega R^2 C}{I + (\omega RC)^2} \tag{7}$$

In Eqs. (6) and (7), R indicates the resistance of the resistance element, C indicates the capacitance of the capacitor element, and $\omega = 2\pi f$, f is the frequency speed of the sine wave.

3. Results and Discussion

3.1 Electrochemical Test Results

3.1.1 Polarization Curve Results

Figures 2 and 3 show that the corrosion potential of the coated steel bar was much larger than that of bare steel, and from the calculation result of the corrosion current density in Fig. 4, that of the coated steel bar was much smaller than that of bare steel, which shows that the coating had a good protective effect on the steel bar. This had the same effect as that when Xiong et al.

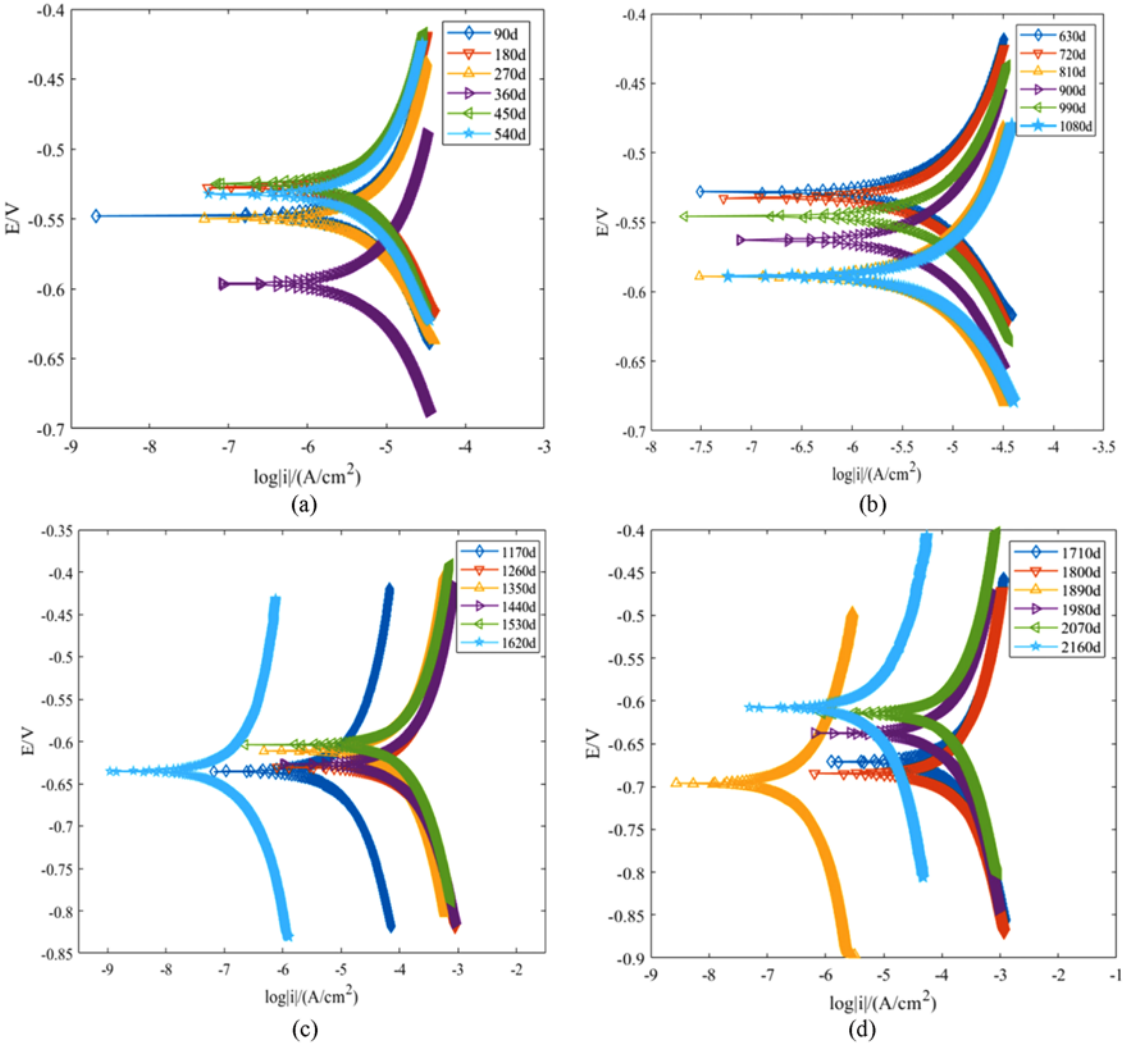

Fig. 2. Polarization Curve from 90d to 2,160d of Group A: (a) Polarization Curve from 90d to 540d, (b) Polarization Curve from 630d to 1,080d, (c) Polarization Curve from 1,170d to 1,620d, (d) Polarization Curve from 1,710d to 2,160d

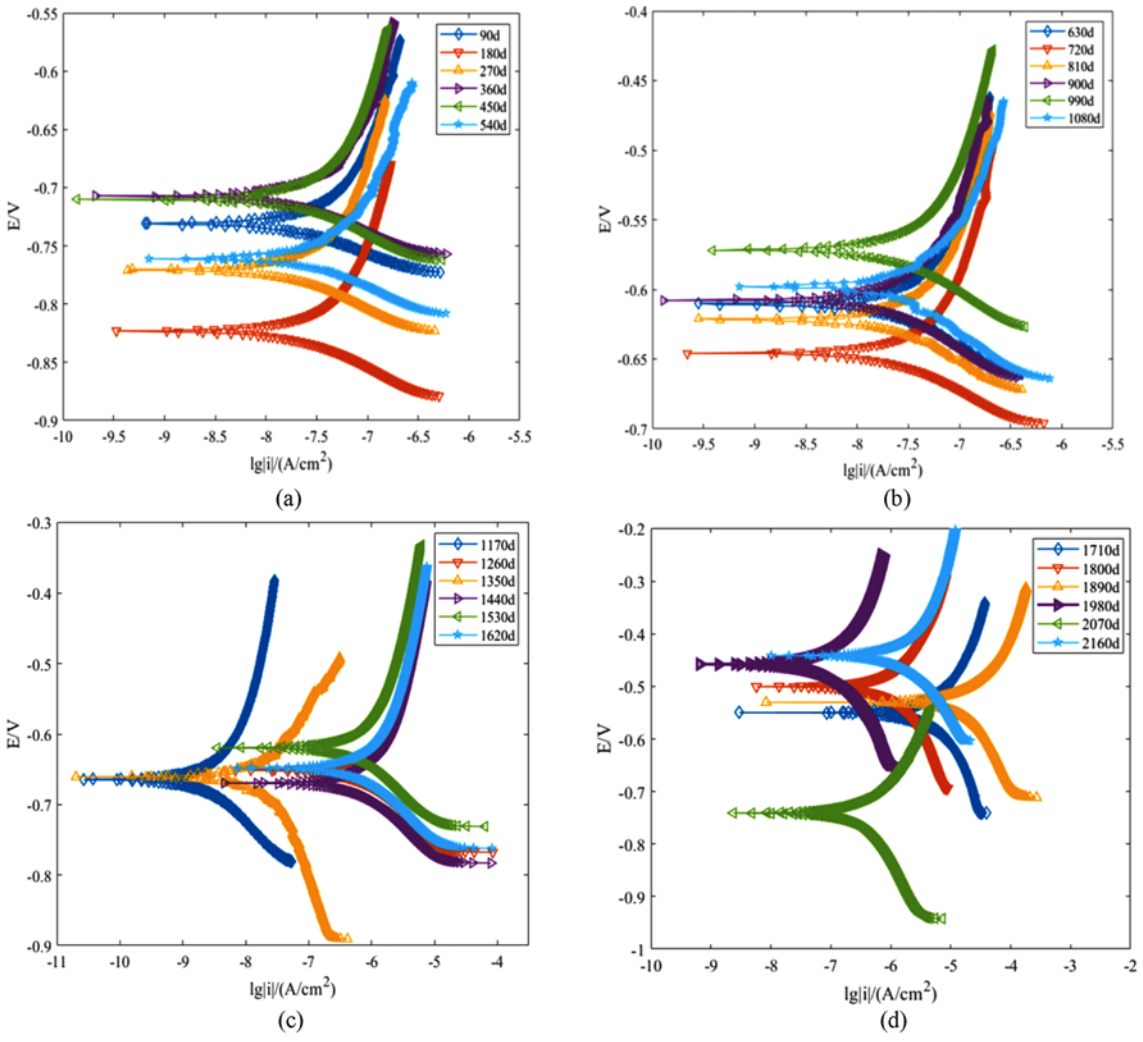

Fig. 3. Polarization Curve from 90d to 2,160d of Group B: (a) Polarization Curve from 90d to 540d, (b) Polarization Curve from 630d to 1,080d, (c) Polarization Curve from 1,170d to 1,620d, (d) Polarization Curve from 1,710d to 2,160d

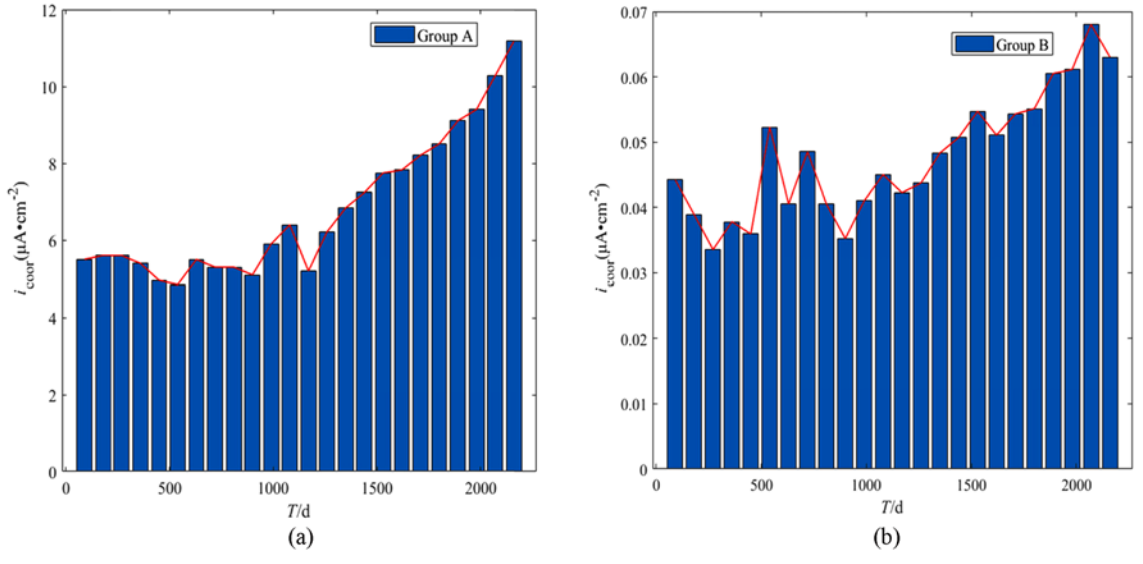

Fig. 4. Corrosion Current Density in Each Period: (a) Corrosion Current Density of Group A, (b) Corrosion Current Density of Group B

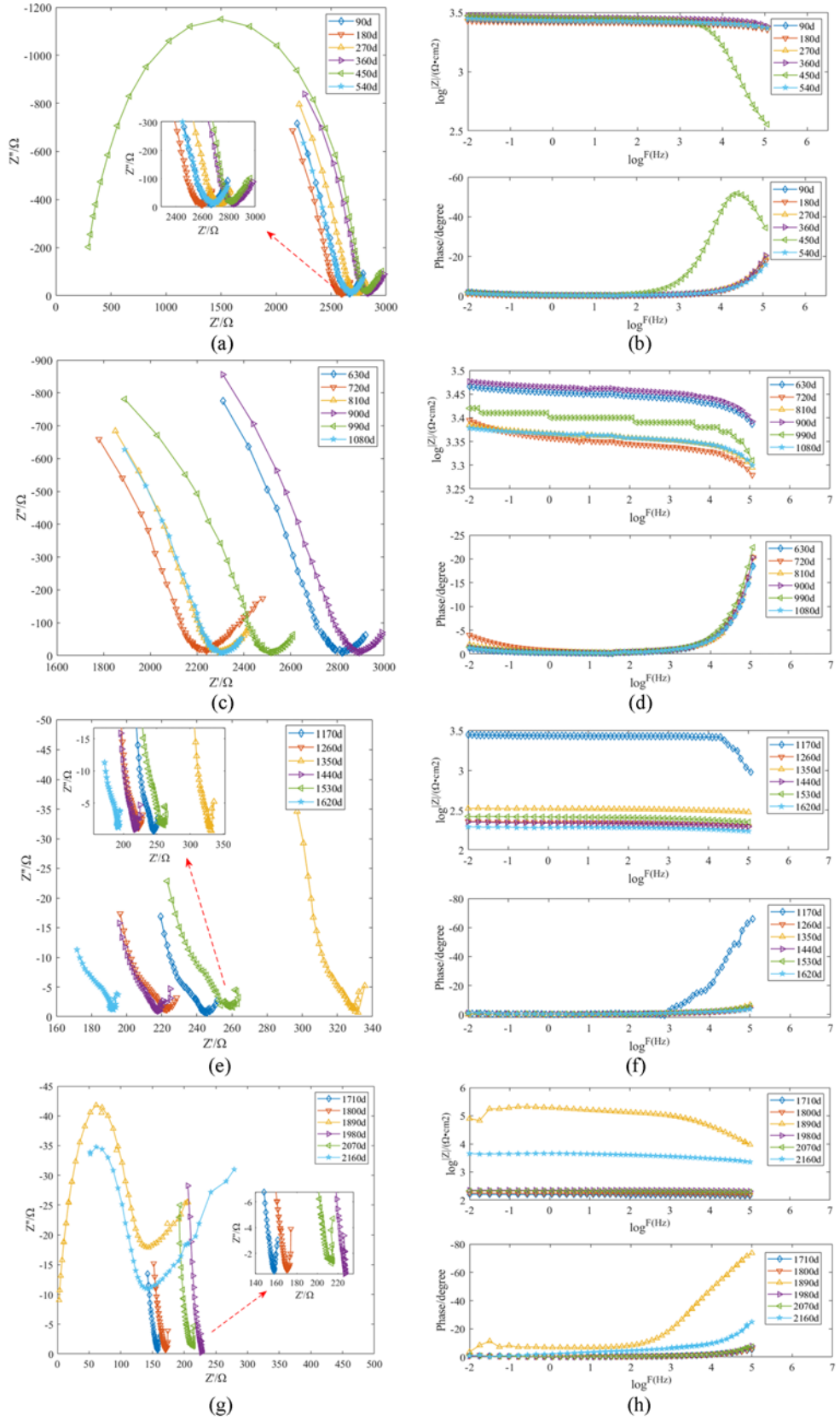

Fig. 5. AC Impedance of Group A in Each Period: (a) -Nyquist Plot from 90d to 540d, (b) Bode Plot from 90d to 540d, (c) -Nyquist Plot from 630d to 1,080d, (d) Bode Plot from 630d to 1,080d, (e) -Nyquist Plot from 1,170d to 1,620d, (f) Bode Plot from 1,170 to 1,620d, (g) -Nyquist Plot from 1,710d to 2,160d, (h) Bode Plot from 1,710d to 2,160d

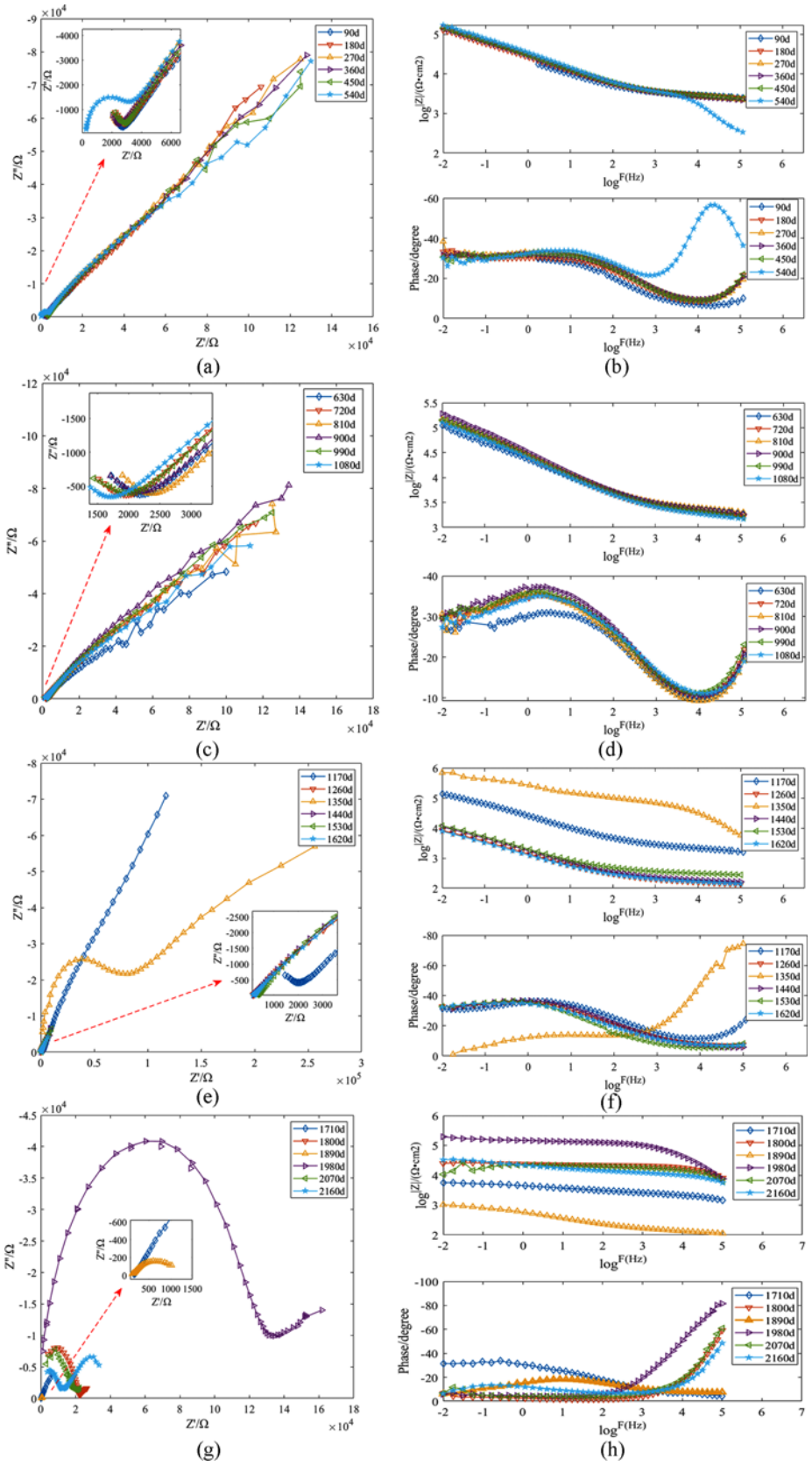

Fig. 6. AC Impedance of Group B in Each Period: (a) -Nyquist Plot from 90d to 540d, (b) Bode Plot from 90d to 540d, (c) -Nyquist Plot from 630d to 1,080d, (d) Bode Plot from 630dto 1,080d, (e) -Nyquist Plot from 1,170d to 1,620d, (f) Bode Plot from 1,170 to 1,620d, (g) -Nyquist Plot from 1,710d to 2,160d, (h) Bode Plot from 1,710d to 2,160d

(2018) used phytic acid conversion coating to protect steel bars, and Ohba et al. (2019) used galvanized zinc to do so. In the polarization curves of the bare and coated steel bars, the Tafel slope of the anode polarization curve of the coated steel bars was larger than that of bare steel at the same time. This was the case because the sacrificial anode effect of the coating provides the steel bars with cathodic protection (Yu et al., 2019). The essence of the protection provided by the steel coating is that the corrosion potential of Zn in the coating is -0.762V, while that of Al is -1.662V, and the natural corrosion potential of both are lower than that of Fe -0.440V (Ohba et al., 2019). It can be seen in Fig. 4 that the corrosion current density of the coated steel bar fluctuated, and both positive and negative movements of the corrosion potential of the coated steel bar occurred. The reason for this is that coating corrosion and the formation of basic zinc carbonate ($Zn_5(OH)_6(CO_3)_2$ and basic aluminum chloride ($Al_5Cl_3(OH)_{12}\cdot 4H_2O$) took place that blocked the coating pores. The chemical equation of this reaction process is shown below:

$$5Zn(OH)_2+2HCO_3^{2-}+2H^+\rightarrow Zn_5(OH)_6(CO_3)_2+4H_2O \quad (8)$$

$$5Al(OH)_3+4H_2O+3Cl^-\rightarrow Al_5Cl_3(OH)_{12}\cdot 4H_2O+3OH^- \quad (9)$$

For bare steel, the fluctuation in the corrosion current density and the positive and negative movements of the corrosion potential are caused by rust's blocking effect and further corrosion that leads to the loss of the rust blocking effect (Wu et al., 2018; Tao et al., 2012).

3.1.2 AC Impedance Results

Figures 5 and 6 are the -Nyquist and Bode diagrams of bare and coated steel bars in different solution immersion stages. -Nyquist represents the corrosion of steel bars largely by measuring the capacitance or polarization impedance in the system, while the Bode diagram represents primarily the position at which the corrosion occurs by the number of time parameters and the movement in the high, medium, and low frequency areas (Fajardo et al., 2019). The -Nyquist diagrams in Figs. 5 and 6 show that for bare steel, the high-frequency area is a semicircular arc, while the low-frequency area is a short arc with a very short tail that is an approximately 45° straight line, while the low-frequency area of the coated steel is an arc with a very long tail that is an approximately 45° straight line, indicating that the bare steel bar is corroded severely, while the coated steel bar is corroded and diffused (Benarioua et al., 2019). From the Bode diagram in Figs. 5 and 6, it can be concluded that there is only one time parameter for the bare steel bar at the beginning of the entire immersion, which occurs at $10^4 - 10^5$ HZ, while the time parameter for the coated steel bar shifts between $10^0 - 10^1$ HZ and $10^4 - 10^5$ HZ, and the corrosion of the bare steel bar's surface occurs within the rust, while that of the coated steel bar occurs on the surface and within the coating (Rengaraju et al., 2019). Fig. 7 shows that the polarization impedance of both the coated and bare steel increased and decreased in the degradation process, but decreased as a whole. This phenomenon is consistent with Fajardo's et al. (2019) research on the corrosion behavior of WIP Fe-Mn-Al-Si original steel in chloride solution and Rengaraju's et al. (2019) study of the corrosion behavior of steel bars in ordinary concrete and fly ash concrete.

3.2 Wiener Degradation

3.2.1 Relevant Knowledge of the Univariate Wiener Process

The univariate Wiener can be expressed as in Sun et al. (2018) and Zhang et al. (2018):

$$X(t,\mu,\sigma^2)=\mu t+\sigma W(t) \quad (10)$$

in which, t is time, μ is the drift parameter, σ is the diffusion

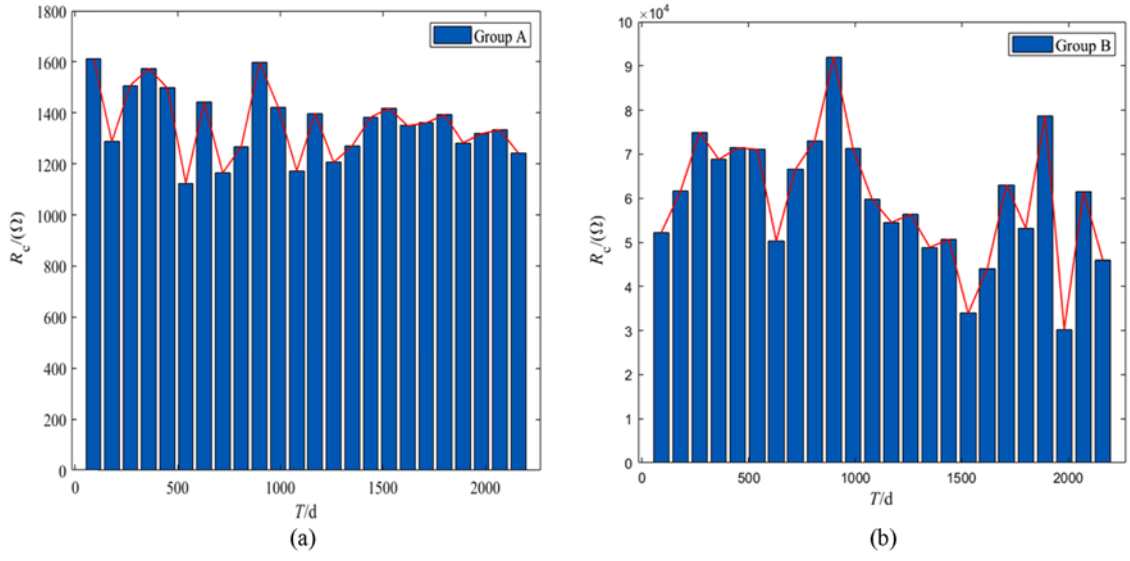

Fig. 7. Polarization Impedance Each Period: (a) Polarization Impedance of Group A, (b) Polarization Impedance of Group B

Table 4. Corrosion Current Density Increment of Coated Steel Bar (μA·cm^{-2})

Parameter	$\Delta_{t1\text{-}t0}$	$\Delta_{t2\text{-}t1}$	$\Delta_{t3\text{-}t2}$	$\Delta_{t4\text{-}t3}$	$\Delta_{t5\text{-}t4}$	$\Delta_{t6\text{-}t5}$	$\Delta_{t7\text{-}t6}$	$\Delta_{t8\text{-}t7}$	$\Delta_{t9\text{-}t8}$	$\Delta_{t10\text{-}t9}$	$\Delta_{t11\text{-}t0}$	$\Delta_{t12\text{-}t11}$
Δi_{coor}	0.0197	-0.0053	-0.0054	0.0043	-0.0019	0.00164	-0.0118	0.008	-0.008	-0.0053	0.0058	0.004
Parameter	$\Delta_{t13\text{-}t12}$	$\Delta_{t14\text{-}t13}$	$\Delta_{t15\text{-}t14}$	$\Delta_{t16\text{-}t15}$	$\Delta_{t17\text{-}t16}$	$\Delta_{t18\text{-}t17}$	$\Delta_{t19\text{-}t18}$	$\Delta_{t20\text{-}t19}$	$\Delta_{t21\text{-}t20}$	$\Delta_{t22\text{-}t21}$	$\Delta_{t23\text{-}t22}$	$\Delta_{t24\text{-}t23}$
Δi_{coor}	-0.0028	0.0015	0.0046	0.0024	0.004	-0.0037	0.0033	0.0008	0.0054	0.0006	0.0069	-0.005

parameter, $W(t)$ is the standard Brownian motion, $E(W(t)) = 0$, $E[W(t_1)W(t_2)] = \min(t_1, t_2)$,

And the one-dimensional, continuous-time stochastic process $[X(t), t \geq 0]$ satisfies the following properties:

1. The increment between time t and time $t+\Delta t$ obeys the normal distribution, in that $\Delta X = X(t + \Delta t) - X(t) \sim N(\mu\Delta t, \sigma^2\Delta t)$;
2. For any two disjoint time regions $[t_1, t_2]$, $[t_3, t_4]$, increments $X(t_4)-X(t_3)$ and $X(t_2)-X(t_1)$ are independent, and
3. $X(0) = 0$ and $X(t)$ is continuous at $t = 0$.

The definition of the stochastic processes $\{Z(t); t > 0\}$ on the basis of univariate Wiener processes, $X(t)$, is that, at any time t ($t \geq 0$), and $Z(t)$ takes $X(t)$ to obtain the maximum value in time $[0, t]$.

$$Z(t) = \sup_{0 \leq s \leq t} \{X(s); s \geq 0\} \tag{11}$$

The probability density function of $Z(t)$ at time t is $g(z, t)$. The definition of $Z(t)$ shows that it is a monotonic stochastic process, and the probability that the product will not fail in time t is:

$$P\{T > t\} = P\{Z(t) < l\} = \int_{-\infty}^{l} g(z,t)dz \tag{12}$$

Cox and Miller (1966) used the Fokker-Planck equation to obtain the expression of $g(z, t)$, as follows:

$$g(z,t) = \frac{1}{\sigma\sqrt{2\pi t}}\left\{\exp\left[\frac{(z-\mu t)^2}{2\sigma^2 t}\right] - \exp\left(\frac{2\mu l}{\sigma^2}\right)\exp\left[-\frac{(z-2l-\mu t)}{2\sigma^2 t}\right]\right\} \tag{13}$$

Add Eq. (13) to Eq. (12) to obtain the reliability function and probability density distribution function, as shown in Eqs. (14) and (15).

$$R(t) = P\{T > t\} = 1 - F(t) = \Phi\left(\frac{l-\mu t}{\sigma\sqrt{t}}\right) - \exp\left(\frac{2\mu l}{\sigma^2}\right)\Phi\left(\frac{-l-\mu t}{\sigma\sqrt{t}}\right) \tag{14}$$

$$f(t) = \frac{l}{\sqrt{2\pi\sigma^2 t^3}}\exp\left[-\frac{(l-\mu t)^2}{2\sigma^2 t}\right] \tag{15}$$

in which l is the failure threshold value.

3.2.2 Wiener Process Modeling Steps

According to the definition of the univariate Wiener and its properties, the life prediction of coated steel bars in magnesium oxychloride cement concrete is carried out in the following steps:

1. Verify whether the corrosion current density increment of coated steel bar obeys a normal distribution;
2. The corrosion threshold is determined according to the corresponding relation between the corrosion current density and the steel bar's corrosion state;
3. Perform parameter estimation and derive a reliability function graph.

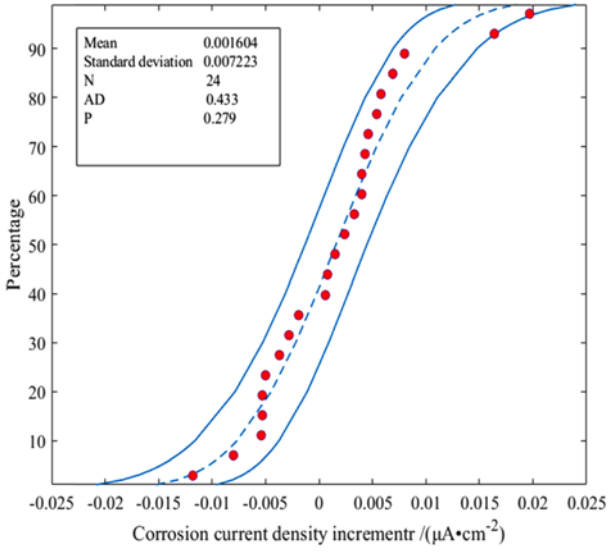

Fig. 8. Normal Distribution Test Chart

3.2.3 Wiener Degradation Process Test

The life prediction of coated steel bars was then carried out. The corrosion current density increment is as follows:

Hypothesis testing was then used to test the distribution of the corrosion current density of the coated steel bars with a confidence level of $\alpha = 0.05$. As Fig. 8 shows, each data point was within the 95% confidence interval. The probability of accepting the hypothetical function was $p = 0.279 > 0.05$. The results showed that the corrosion current density of coated steel bars obeyed the normal distribution.

3.2.4 Parameter Estimation

From the probability density function in Eq. (15), we can see that the maximum likelihood function of the probability density at a certain time is:

$$L(\mu, \sigma^2) = \prod_{i=1}^{n}\prod_{j=1}^{m_i}\frac{1}{\sqrt{2\sigma^2\pi\Delta t_{ij}}}\exp\left[-\frac{(\Delta x_{ij}-\mu\Delta t_{ij})}{2\sigma^2\Delta t_{ij}}\right] \tag{16}$$

The maximum likelihood estimates of parameter μ, σ can be

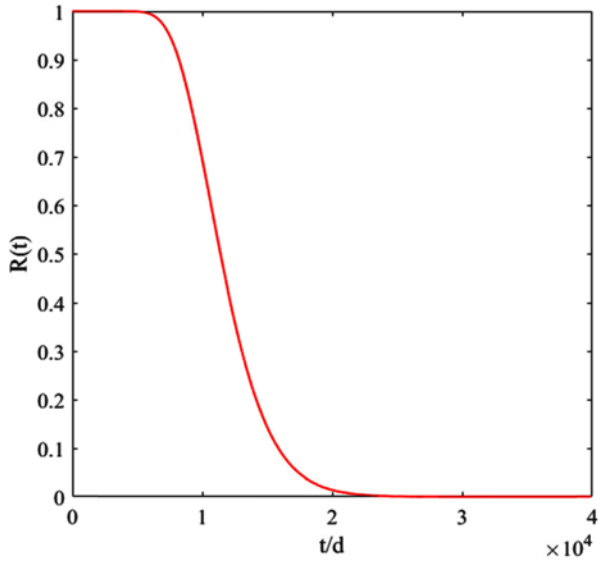

Fig. 9. Reliability Map of Coated Steel Bars

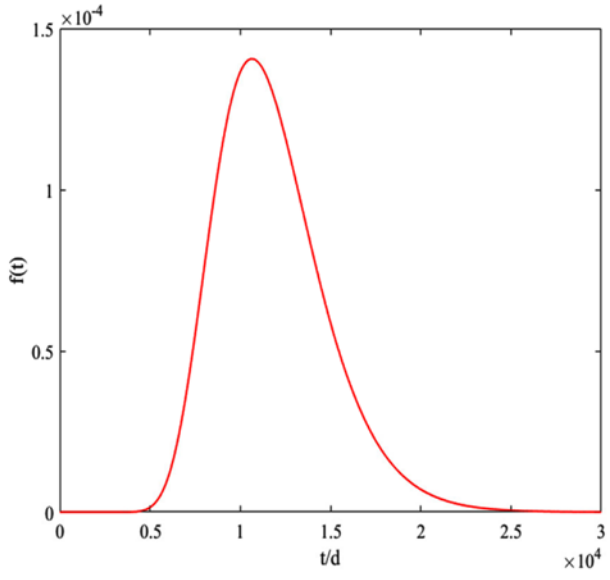

Fig. 10. Density Function Diagram of Coated Steel Bars

obtained by taking the logarithm of Eq. (16) and calculating the partial derivatives of μ, σ, respectively.

$$\hat{\mu}=\frac{\sum_{i=1}^{n} X_{im_i}}{\sum_{i} t_{im_i}}, \hat{\sigma}^2=\frac{1}{\sum_{i=1}^{n} m_i}\left[\sum_{i=1}^{n}\sum_{j=1}^{m_i}\frac{(\Delta X_{ij})^2}{\Delta t_{ij}}-\frac{\left(\sum_{i=1}^{n} X_{im_i}\right)^2}{\sum_{i=1}^{n} t_{im}}\right] \tag{17}$$

in which, i = 1, 2, 3… n, j = 1, 2, 3…m_i, i is the number of specimen, j is the number of tests, X_{im_i} is the deterioration of product performance at a given time, $\Delta X_{ij}= X_{ij}-X_{i(j-1)}$, $\Delta t_{ij}= t_{ij}-t_{i(j-1)}$; $\hat{\mu}$ = 0.000042444 and $\hat{\sigma}^2 = 1.4333\times10^{-6}$ are calculated. The expressions of the reliability and probability density functions are as follows:

$$R(t)=\Phi\left(\frac{0.5-0.000042444t}{1.197\times10^{-3}\sqrt{t}}\right)-\exp(29.612)\,\Phi\left(\frac{-0.5-0.000042444t}{1.197\times10^{-3}\sqrt{t}}\right) \tag{18}$$

$$f(t)=\frac{0.5}{\sqrt{2\pi1.4333\times10^{-6}t^{-3}}}\exp\left(-\frac{(0.5-0.000042444t)^2}{2\times1.4333\times10^{-6}t}\right) \tag{19}$$

in which, $\Phi(x)$ is the standard normal distribution function.

By using the expressions of the reliability function and probability densityin MATLAB software, the results are shown in Figs. 9 and 10.

Figure 9 shows that the reliability was 1 to 5,401 days, indicating that the coating protected the steel from corrosion well at this stage. After 5,401 days, the reliability decreased gradually, and reached zero at 21,800 days, indicating that the coating lost its protective effect on the steel at 21,800 days. To ensure that the coating has highly reliable protective performance, the time at $R_{0.6}(t)$ is generally taken as the coating's failure time (the corresponding time when the reliability decreases by 40% or reaches 60%), in which the $R_{0.6}(t)$ was 10,650 days.

4. Conclusions

The solution immersion test was used in this paper to accelerate the degradation of coated steel in MOCC, and the electrochemical workstation was used to track and detect the degradation process of steel bars in the specimen. Based on the Wiener degradation process, the corrosion of the coated steel bars was predicted to investigate whether the coating can provide long-term, stable protection of steel bars in MOCC. The conclusions are as follows:

1. The polarization curve shows that the Tafel slope of the anode polarization curve of a coated steel bar was always very large throughout the process of immersion in solution. From the -Nyquist and Bode diagrams, it can be seen that only a single time parameter was generated and disappeared quickly, indicating that the coating was stable in the process of providing protection for the steel bar.
2. The coating was able to protect the steel bar in MOCC from corrosion. After 2.160 days of immersion in the accelerated corrosion test, the corrosion current density of the coated steel bars was 0.063 μA·cm^{-2}, such that they were still in a state of non-corrosion.
3. The corrosion current density of bare steel showed a stable growth trend throughout the soaking process, while that of the coated steel bars also showed a growth trend in the soaking process, although it decreased in some periods. However, the polarization impedance of bare steel and coated steel decreased throughout the immersion process.
4. It is feasible to take the corrosion current density of the coated steel bar as the degradation parameter to model based on the Wiener function. After calculation, it was concluded finally that the coated steel bar reached the limit of severe corrosion at approximately 21,800d and $R_{0.6}(t)$ = 10,650d.

Acknowledgements

This work was financially supported by the National Natural Science Foundation of China (Nos. 51468039, 51868044). This Paper is Funded by Hongliu First-class Discipline Construction Program of Lanzhou University of Technology. Authors appreciate the financial and equipment supports.

ORCID

Penghui Wang https://orcid.org/0000-0001-8704-5786
Hongxia Qiao https://orcid.org/0000-0002-0289-1949
Kefan Chen https://orcid.org/0000-0003-4664-3282
Yuanke Li https://orcid.org/0000-0002-6797-9159
Qiong Feng https://orcid.org/0000-0002-4298-6248

References

Benarioua M, Mihi A, Bouzeghaia N, Naoun M (2019) Mild steel corrosion inhibition by Parsley (Petroselium Sativum) extract in acidic media. *Egyptian Journal of Petroleum* 28(2):155-159, DOI: 10.1016/j.ejpe.2019.01.001

Chau CK, Chan J, Li ZJ (2009) Influences of fly ash on magnesium oxychloride mortar. *Cement and Concrete Composites* 31(4):250-254, DOI: 10.1016/j.cemconcomp.2009.02.011

Cox DR, Miller HD (1966) The theory of stochastic processes. *Physics Today* 19(12):81-83, DOI: 10.1063/1.3047872

Fajardo S, Llorente I, Jiménez JA, Bastidas JM, Bastidas DM (2019) Effect of Mn additions on the corrosion behaviour of TWIP Fe-Mn-Al-Si austenitic steel in chloride solution. *Corrosion Science* 154:246-253, DOI: 10.1016/j.corsci.2019.04.026

Gong W (2017) Experiment on steel reinforcement anti-corrosion in magnesium oxychloride cement concrete and comprehensive evaluation. MSc Thesis, Lanzhou University of Technology, Lanzhou, China (in Chinese)

Hu YG, Li H, Shi PP, Chai ZS, Chen Z (2018) A prediction method for the real-time remaining useful life of wind turbine bearings based on the Wiener process. *Renewable Energy* 127:452-460, DOI: 10.1016/j.renene.2018.04.033

Hu CL, Xu BW, Ma HY, Chen BM, Li ZJ (2016) Micromechanical investigation of magnesium oxychloride cement paste. *Construction and Building Materials* 105:496-502, DOI: 10.1016/j.conbuildmat.2015.12.182

JGJ63-2006 (2018) Standard of water for concrete. Ministry of Construction of the People's Republic of China, Beijing, China

Jin ZQ, Sun W, Zhang YS, Jiang JY, Lai JZ (2007) Interaction between sulfate and chloride solution attack of concretes with and without fly ash. *Cement and Concrete Research* 37(8):1223-1232, DOI: 10.1016/j.cemconres.2007.02.016

Li ZJ, Chau CK (2007) Influence of molar ratios on properties of magnesium oxychloride cement. *Cement and Concrete Research* 37(6):866-870, DOI: 10.1016/j.cemconres.2007.03.015

Li NP, Gebraeel N, Lei Y, Bian LK, Si XS (2019) Remaining useful life prediction of machinery under time-varying operating conditions based on a two-factor state-space model. *Reliability Engineering & System Safety* 186:88-100, DOI: 10.1016/j.ress.2019.02.017

Ma HY, Gong W, Yu HF, Sun W (2018) Durability of concrete subjected to dry-wet cycles in various types of salt lake brines. *Construction & Building Materials* 193:286-294, DOI: 10.1016/j.conbuildmat.2018.10.211

Mohabbi M (2019) Investigation of sulfates effects in perlite-based geopolymer. *Structural Concrete* 20(4):1402-1410, DOI: 10.1002/suco.201900039

Ohba M, Scarazzato T, Espinosa DCR, Panossian Z (2019) Study of metal electrodeposition by means of simulated and experimental polarization curves: Zinc deposition on steel electrodes. *Electrochimica Acta* 309:86-103, DOI: 10.1016/j.electacta.2019.04.074

O'Reilly M, Farshadfar O, Darwin D, Browning J, Locke CEJr (2018) Corrosion-induced concrete cracking for uncoated and galvanized reinforcing bars. *ACI Materials Journal* 115(6):825-832, DOI: 10.14359/51706839

Qiao HX, Zhu BR, Feng Q, Desire N, Dong JM (2018) Accelerated life testing of reinforced concrete based on performance degradation and reliability modeling. *Journal of Materials in Civil Engineering* 30(5), DOI: 10.1061/(ASCE)MT.1943-5533.0002225

Rengaraju S, Neelakantan L, Pillai RG (2019) Investigation on the polarization resistance of steel embedded in highly resistive cementitious systems - An attempt and challenges. *Electrochimica Acta* 308:131-141, DOI: 10.1016/j.electacta.2019.03.200

Skalny JP (2000) Special inorganic cements. *Cement and Concrete Research* 30(9):1511-1511, DOI: 10.1016/S0008-8846(00)00369-0

Sotiriadis K, Mróz R (2019) Simulation of thaumasite sulfate attack on portland cement mixtures using synthesized cement phases. *Journal of Materials in Civil Engineering* 31(12), DOI: 10.1061/(ASCE)MT.1943-5533.0002612

Sun HB, Cao DaL, Zhao ZD, Kang X (2018) A hybrid approach to cutting tool remaining useful life prediction based on the wiener process. *IEEE Transactions on Reliability* 67(3):1294-1303, DOI: 10.1109/TR.2018.2831256

Tan YN, Liu Y, Grover L (2014) Effect of phosphoric acid on the properties of magnesium oxychloride cement as a biomaterial. *Cement and Concrete Research* 56(2):69-74, DOI: 10.1016/j.cemconres.2013.11.001

Tang FJ, Chen G, Richard KB (2016) Chloride-induced corrosion mechanism and rate of enamel- and epoxy-coated deformed steel bars embedded in mortar. *Cement and Concrete Research* 82:58-73, DOI: 10.1016/j.cemconres.2015.12.015

Tao Z, He W, Wang S, Zhang S, Zhou G (2012) A study of differential polarization curves and thermodynamic properties for mild steel in acidic solution with nitrophenyltriazole derivative. *Corrosion Science* 60:205-213, DOI: 10.1016/j.corsci.2012.03.035

Wang JB, Niu DT, Wang Y, Wang B (2018) Durability performance of brine-exposed shotcrete in salt lake environment. *Construction and Building Materials* 188:520-536, DOI: 10.1016/j.conbuildmat.2018.08.139

Wang YC, Wei LZ, Yu JT, Yu KQ (2019) Mechanical properties of high ductile magnesium oxychloride cement-based composites after water soaking. *Cement and Concrete Composites* 97:248-258, DOI: 10.1016/j.cemconcomp.2018.12.028

Wei LZ, Wang YC, Yu, JT (2018) Feasibility study of strain hardening magnesium oxychloride cement-based composites. *Construction and Building Materials* 165:750-760, DOI: 10.1016/j.conbuildmat.2018.01.041

Wu J, Dong L, Deng JH, Hou D, Li GZ, Li DJ, Xue WB (2018) Direct growth of oxide layer on carbon steel by cathodic plasma electrolysis. *Surface and Coating Technology* 338:63-68, DOI: 10.1016/j.surfcoat.2018.01.080

Xiong CS, Li WH, Jin ZQ, Gao X (2018) Preparation of phytic acid

conversion coating and corrosion protection performances for steel in chlorinated simulated concrete pore solution. *Corrosion Science* 139:275-288, DOI: 10.1016/j.corsci.2018.05.018

Yehia S, Farrag S, Abdelghaney O (2019) Performance of fiber-reinforced lightweight self-consolidating concrete exposed to wetting-and-drying cycles in salt water. *ACI Materials Journal* 116(6):45-54, DOI: 10.14359/51716976

Yu JH, Zhang YF, Jin XY, Chen L, Xue WB (2019) Fabrication and optical emission spectroscopy of enhanced corrosion-resistant CPEO films on Q235 low carbon steel. *Surface and Coatings Technology* 363:411-418, DOI: 10.1016/j.surfcoat.2019.02.073

Zhang D, Shao Y, Zhang D, Cai X, Jaworska B, Zhang D, Li VC, Ellis BR (2019) Enhancing chloride corrosion resistance of precast reinforced concrete by carbonation curing. *ACI Materials Journal* 116(3):3-12, DOI: 10.14359/51714461

Zhang ZX, Si XS, Hu CH, Lei YG (2018) Degradation data analysis and remaining useful life estimation: A review on Wiener-process-based methods. *European Journal of Operational Research* 271:775-796, DOI: 10.1016/j.ejor.2018.02.033